Materials Today Bio 23 (2023) 100799

Contents lists available at ScienceDirect

Materials Today Bio

journal homepage: www.journals.elsevier.com/materials-today-bio

Advantages of photo-curable collagen-based cell-laden bioinks compared to methacrylated gelatin (GelMA) in digital light processing (DLP) and extrusion bioprinting

Huimin Shi [a,b,1], Yang Li [a,c,1], Kailei Xu [d,e,f,*], Jun Yin [a,b,**]

[a] The State Key Laboratory of Fluid Power and Mechatronic Systems, School of Mechanical Engineering, Zhejiang University, Hangzhou, 310027, China
[b] Key Laboratory of 3D Printing Process and Equipment of Zhejiang Province, School of Mechanical Engineering, Zhejiang University, Hangzhou, 310027, China
[c] Key Laboratory of Soft Machines and Smart Devices of Zhejiang Province, Department of Engineering Mechanics, Zhejiang University, Hangzhou, 310027, China
[d] Department of Plastic and Reconstructive Surgery, The First Affiliated Hospital, Ningbo University School of Medicine, Ningbo, 315010, China
[e] Center for Medical and Engineering Innovation, Central Laboratory, The First Affiliated Hospital, Ningbo University School of Medicine, Ningbo, 315010, China
[f] Key Laboratory of Precision Medicine for Atherosclerotic Diseases of Zhejiang Province, Ningbo, 315010, China

ARTICLE INFO

Keywords:
Methacrylated gelatin
Photo-curable collagen
Cell-laden bioink
3D bioprinting

ABSTRACT

The development of cell-laden bioinks that possess high biocompatibility and printability is crucial in the field of bioprinting for the creation of cell-embedded tissue engineering scaffolds. As widely known, methacrylated gelatin (GelMA) is one of the most commonly used photo-crosslinkable bioink for cell-laden bioprinting with different printing methods, but GelMA is the derivative of gelatin, so it loses the unique triple-helix molecular structure of collagen and may not be able to successfully activate the cellular pathways or facilitate cell-matrix interaction as effectively as collagen. Recently, methacrylated collagen (CMA) was developed to be an alternative photocrosslinkable bioink with a good bioactivity, but its low printability and biocompatibility limited that application in tissue engineering. In this study, the synthetic process for CMA was improved by synthesizing under 4 °C and using acidic aqueous solution as solvent. Our CMA bioinks were demonstrated a similar printability as GelMA in extrusion bioprinting, while a better formability in digital light processing (DLP). To further analyze the bioactive properties, CMA bioinks were encapsulated with Schwann cells (SCs) and bone mesenchymal stem cells (BMSCs) for printing. SCs-laden CMA bioinks had a significantly higher proliferation rate and expression of neural stem cell-associated genes than GelMA in DLP bioprinting. While, BMSCs-laden CMA bioinks demonstrated >95% cellular viability, better cell spreading and higher expression of osteogenesis-related genes than that of GelMA. Overall, we speculate that the CMA-based bioink developed in this study could be potential bioinks for 3D cell-laden bioprinting in the future.

1. Introduction

Three-dimensional (3D) cell-laden scaffolds are of great significance in tissue engineering. Encapsulating cells or tissue-inducing substances such as growth factors in scaffolds can precisely distribute cells or tissue-inducing substances on demand during printing and increase the retention rate of the cells or substances during body fluid circulation [1,2]. These advantages overcome the limitations of other conventional scaffold manufacturing methods, including direct injection or seeding cells on the surface of scaffolds [3]. 3D cell-laden bioprinting is an appropriate technology to encapsulate cells in scaffolds, which can simultaneously support and resemble native tissues [4–6], because cells are kept alive during 3D bioprinting [7] by precisely controlling the pore size [8]. The main technologies of 3D cell-laden bioprinting are inkjet bioprinting [9,10], extrusion bioprinting [11,12], and stereolithography bioprinting [13–15]. Soft biomaterials loaded with living cells are

* Corresponding author. Department of Plastic and reconstructive surgery, the First Affiliated Hospital, Ningbo University School of Medicine, Ningbo, 315010, China.
** Corresponding author. The State Key Laboratory of Fluid Power and Mechatronic Systems, School of Mechanical Engineering, Zhejiang University, Hangzhou, 310027, China.
E-mail addresses: xukailei@zju.edu.cn (K. Xu), junyin@zju.edu.cn (J. Yin).
[1] These authors contributed equally to this work.

https://doi.org/10.1016/j.mtbio.2023.100799
Received 16 May 2023; Received in revised form 5 September 2023; Accepted 14 September 2023
Available online 16 September 2023

referred as "bioink" and are the indispensable "raw materials" for all cell-laden bioprinting techniques. Bioinks have been developed to manipulate biological environments and living cells to create complex, cell-laden constructs. Sustained cell viability during printing and during short- and long-term culture after printing, as well as cell spreading, proliferation, and functionality, are essential for bioink application. The bioinks used in inkjet bioprinting have low viscosity, rheological behavior, and medium surface tension, while those used in extrusion bioprinting exhibit shear thinning behavior, rapid gelation, and shape retention. Bioinks used in stereolithography bioprinting have good photo-crosslinking properties, low toxicity photo-initiators, and retention of uniform cell distribution [16]. Thus, the bioink used in 3D cell-laden bioprinting should have perfect cytocompatibility, proper rheology, and crosslinking mechanisms.

Recently, photo-crosslinkable biomaterials are popular bioinks for 3D bioprinting. Compared with synthetic polymers (poly (ethylene glycol) diacrylate [17], photo-crosslinkable resins [18], etc.), derivatives of natural compounds, such as methacrylated gelatin (GelMA, a derivative of gelatin) is commonly used as cell-laden bioink materials, contain arginine-glycine-aspartic acid (RGD) sequences that promote cell adhesion and possess excellent biocompatibility. But, it is worth noting that gelatin is a partially hydrolyzed product of collagen that has been denatured by heating, which loses the unique triple-helix molecular structure of collagen [19] and GelMA as its derivative also loses the structure. Collagens are the main component of the extracellular matrix and major structural proteins that comprise approximately 30% of total protein in the human or animal body [20]. Moreover, the collagen molecule contains not only RGD sequences but also the polypeptide sequence Gly–Pro–Hyp (GPO) [21] and Gly Phe-Hyp (GFO) [22] motifs in their typical triple helix α-peptide chains, which activate signals and facilitate communication between cells and this is what gelatin and its derivatives cannot provide. Thus, it is more promising to develop collagen-based bioinks for 3D bioprinting on the basis of preserving the typical triple-helix molecular structure.

Salt-soluble and enzyme-soluble collagens account for the majority of collagens (such as type I collagen derived from pig skin or bovine tendon), may partially lose telopeptides from collagen molecules [23], which has major effects on fibril growth [24] and are not able to form hydrogels. For acid-soluble collagens, such as type I collagen extracted from rat tails, can self-assemble [25] and form hydrogels by diffusion-limited aggregation [26,27], which is accomplished by adjusting the pH value of the solution to 6.5–8.5. However, the diffusion-driven crosslinking process takes at least 20 min to complete [26], which is too slow to solidify 3D printed constructs, leading to the construct collapse during extrusion bioprinting [28]. The methacrylated collagen (CMA)-based [29,30] bioinks have been developed for 3D printing with much faster photo-curing rate (about 10 s). However, the currently developed CMA bioink has limitations on the printability and cellular viability compared to GelMA bioink, due to the poor water-solubility, rheology and stability caused by fibrous structures and wide sources of collagens. The free-form fabrication of cell-laden CMA through photomasks was previously studied while the printability was still very poor [31]. A dual crosslinking strategy was used to enhance the mechanical rigidity and stability of extrusion-printed acid soluble CMA constructs, while the cell viability was reduced to 50% after 7 days of culture [32]. CMA derived from marine collagen was developed and could be used for coaxial printing, while the cells encapsulated in the printed scaffolds has high death rate [33]. In further, limited studies deeply investigated of the influence for CMA on cellular morphology and gene expression [34], which limited the application of CMA in tissue engineering. The limitations of CMA bioink on the printability and cellar viability may attribute to the diverse resources of collagen and the synthesis protocols for the CMA used in the previous literature [31–33] were acid-soluble so the concentration (2.5–3 mg/mL) was too low to be printed precisely and the synthesis protocol [29,30] may influence the stability or cause organic toxicity [35]. Therefore, it has great value to modify the synthetic process for acid-insoluble CMA and keep the stability of CMA while being synthetized, then improve the printability and biocompatibility in 3D bioprinting and deeply investigate the influence on cellular behavior for the wider application of CMA in tissue engineering.

In this study, type I collagen from porcine skin was modified by methacrylation in an improved method to form CMA. The excellent printability of the CMA bioink with high concentration (15–30 mg/mL), which was solid-liquid mixture containing acid-insoluble CMA, developed in this study was demonstrated using DLP and extrusion printing. The biological properties of CMA bioink was evaluated by encapsulating Schwann cells (SCs) or bone mesenchymal stem cells (BMSCs) during the DLP and extrusion printing. The changes of cellular morphology, proliferation, viability, and gene expression were investigated to compare CMA with GelMA.

2. Materials and methods

2.1. Materials

Type I collagen from porcine skin tissue (100–300 kDa, 1.5 wt% in acetic acid) was purchased from Chengdu Kele Biological Technology Co., Ltd (China). Methacrylic anhydride (MAA M102529), acetic acid (HAc, A116167), gelatin (~250 bloom, G108395), Tris (T274227), β-mercaptoethanol (M301573), and bromophenol blue (B109642) were purchased from Shanghai Aladdin Bio-Chem Technology Co., Ltd. (China). Sodium hydroxide (NaOH, 10019764) and ethanol (100092680) were purchased from Sinopharm Chemical Reagent Co. Ltd. (China). Glycerol (G810575) and sodium dodecyl sulfate (SDS, S817788) were purchased from Shanghai Macklin Biochemical Co., Ltd. (China). Coomassie blue R250 (S19062) was purchased from Shanghai Yuanye Biotechnology Co., Ltd. (China). Alpha-minimum essential medium (αMEM, CR11950) was purchased from Zhejiang Cienry Biotechnology Co., Ltd. (China). Dulbecco's modified Eagle's medium (DMEM, C11995500BT) and fetal bovine serum (FBS, 10099–141) were purchased from GIBCO (USA). Calcein AM (C2012), cell counting kit-8 (CCK-8, C0039), bicinchoninic acid (BCA) protein assay kits (P0012S), Triton X-100 (P0096), 4% paraformaldehyde (PFA) fix solution (P0099), and 2-(4-amidinophenyl)-6-indolecarbamidine dihydrochloride (DAPI) staining solution (C1006) were purchased from Beyotime Biotechnology (China). Propidium iodide (PI, P8080), FITC-phalloidin (CA1620), phosphate-buffered saline (PBS, P1020), and penicillin-streptomycin (P/S, P1400) were purchased from Beijing Solarbio Science & Technology Co., Ltd. (China). Trypsin-EDTA (T6540) was purchased from Shanghai Macklin Biochemical Co. Ltd. (Shanghai, China). GenScript SurePAGE gels (M00652) were purchased from GenScript Biotech Corporation (Beijing, China). Bone mesenchymal stem cells (BMSCs) from Sprague-Dawley rats (RASMX-01001) were obtained from Cyagen Biosciences Inc. (Guangzhou, China). Rat Schwann cells (SCs) were purchased from Procell Life Science and Technology Co., Ltd. (China).

2.2. Synthesis of CMA

We improved the method for synthesizing CMA as above described (Fig. 2a) based on previous studies [29,30]. Type I collagen was diluted 4 × with deionized water and the pH was adjusted to 7.0 with 1.0 M NaOH. The solution was stirred for 30 min at 4 °C. MAA was added to the reaction mixture at a molar ratio of 3:1 (MAA: collagen lysine). After the mixture reacted at 4 °C for 48 h, the solution was dialyzed against 0.5% (v/v) acetic acid using an 8–14 kDa cutoff dialysis tube for 3 days at room temperature, then lyophilized for 2 days. Lyophilized CMA sponges were sterilized with 75% (v/v) ethyl alcohol for 30 min at 25 °C followed by air-drying on a sterile super-clean bench for 12 h. After sterilization, the solid was stored at −20 °C. Methacrylated gelatin (GelMA) with the appropriate degree of methacrylate modification (~30 and ~98%) and lithium phenyl-2,4,

6-trimethylbenzoylphosphinate (LAP) were prepared using the method described in our previous work [11].

2.3. Chemical and structural characterization of CMA

To verify the target product (CMA), ^{1}H-NMR spectra were acquired using a 500 MHz AVANCE III spectrometer (Bruker, Switzerland) at 24 °C using 1 mg/mL native collagen and CMA samples prepared in D_2O with 10 mM deuterium hydrochloric acid (DCl). The methacrylation degree of CMA was quantified using BCA protein assays and 2,4,6- trinitrobenzenesulfonic acid (TNBS) colorimetric assays [35].

Circular dichroism (CD) spectroscopy was performed with a J-1500-150 S T CD Spectrometer (JASCO, Japan) using 0.2 mg/mL native collagen, CMA, gelatin, or GelMA in 0.5% (v/v) acetic acid. Sample solutions were injected into quartz cells (0.1 cm path length). CD spectra were collected between 190 and 260 nm at a scan rate of 1 nm/s. The spectrum of 0.5% (v/v) acetic acid was subtracted from all sample spectra.

SDS-PAGE was performed using a Mini-PROTEAN Tetra electrophoresis tank (Bio-Rad, USA). 2.5 mg/mL native collagen or CMA in 0.5% (v/v) acetic acid was centrifuged at 12,000×*g* for 10 min. The supernatant was mixed with 5 × sample loading buffer containing 10% (w/v) SDS, 50% glycerin (v/v), 0.25% (w/v) bromophenol blue, 1.5% (w/v) Tris base, 1% (v/v) β-mercaptoethanol, and deionized water (pH 6.8) at ratio of 1:4. The mixture was heated for 10 min at 100 °C. Then, 10 μL of each mixture was added to a SurePAGE gel for fractionation (140 V, 1 h). The gel was washed with deionized water three times, stained for 1 h with staining solution containing 0.1% (w/v) Coomassie blue R-250, 40% (v/v) ethanol, and 10% (v/v) acetic acid while shaking, and bleached for 1 h with bleaching solution containing 10% (v/v) ethanol and 7.5% (v/v) acetic acid while shaking. Washing, staining, and bleaching were repeated until the protein bands were visualized. The molecular weights of the protein bands were identified and compared to standard protein molecular weight markers.

2.4. Preparation of CMA-based bioinks

Sterile CMA solid was dissolved in 0.5% (v/v) acetic acid while stirring at 25 °C to form a homogeneous stock suspension, and pH of the suspension was adjusted to 7.2–7.4. Photoinitiator (LAP) or gelatin was then added to the neutral suspension to prepare the target bioinks.

For DLP bioprinting (Fig. 1), CMA suspension at a concentration of 1.5–2.0 wt% (diluted from the stock suspension) with 0.5–1.0 wt% LAP was used as bioink (Table 1). SCs at a final density of 1.0×10^6 cells/mL were incorporated into the CMA suspension to form cell-laden bioinks. 5 wt% GelMA with ~98% methacrylation was dissolved in DMEM complete culture medium, which was used as the control group. The LAP concentration was 0.5 wt%.

For extrusion bioprinting (Fig. 1), 15 wt% gelatin solution was mixed with 5 wt% CMA stock suspension to form CMA/gelatin bioink with different concentration ratios. Blended bioinks contained 1.5–3.0 wt% CMA, 2.5–10 wt% gelatin, and 0.5 wt% LAP (Table 1). BMSCs were used (final density of 1.0×10^6 cells/mL) to prepare cell-laden extrusion bioink. The bioinks were cured by UV light (365 nm, 3 mW/cm^2) at 22 °C for photo-crosslinking.

2.5. Bioink characterization

2.5.1. Rheology

Rheological investigations of the different bioinks were carried out using a rheometer (MCR102, Anton Paar, Austria) equipped with different geometries. The photo-rheological investigations were conducted using a rheometer equipped with a 50 mm diameter cone plate and a light-curing system combined with a UV light source (OmniCure 2000, USA). Changes in storage modulus (G′) and loss modulus (G″) were monitored at a UV light intensity of 1.69 mW/cm^2, while the frequency was maintained at 50 Hz and the strain at 1%. A 25-mm diameter parallel plate was used to measure the G′ and G″ values from 37 °C to 4 °C at a ramp rate of −1 °C/min. The strain was monitored at 1% and frequency at 2 Hz. Viscosity (as a function of temperature) was measured from 37 °C to 4 °C (ramp rate of −1 °C/min) with a constant shear rate of 10 s^{-1}. To ensure the shear thinning behavior of the bioinks, viscosity was tested by varying the shear rate in the range of 1–500 s^{-1} while maintaining the temperature at 22 °C. To study the fast shear recovery performance of bioinks, the viscosity in two repetitive steps was monitored. First, the shear rate was tested at 0.1 s^{-1} for 200 s. Then, the shear rate was changed sharply at a value of 100 s^{-1} for 10 s. Finally, the shear rate was returned to 0.1 s^{-1} for 200 s. All steps were performed at 22 °C. A dynamic stain sweep test was used to determine the self-supporting behavior of the hydrogels. In the dynamic strain sweep, G′ and G″ were measured at a constant frequency of 10 s^{-1} by varying the strain from 0.01% to 1000%.

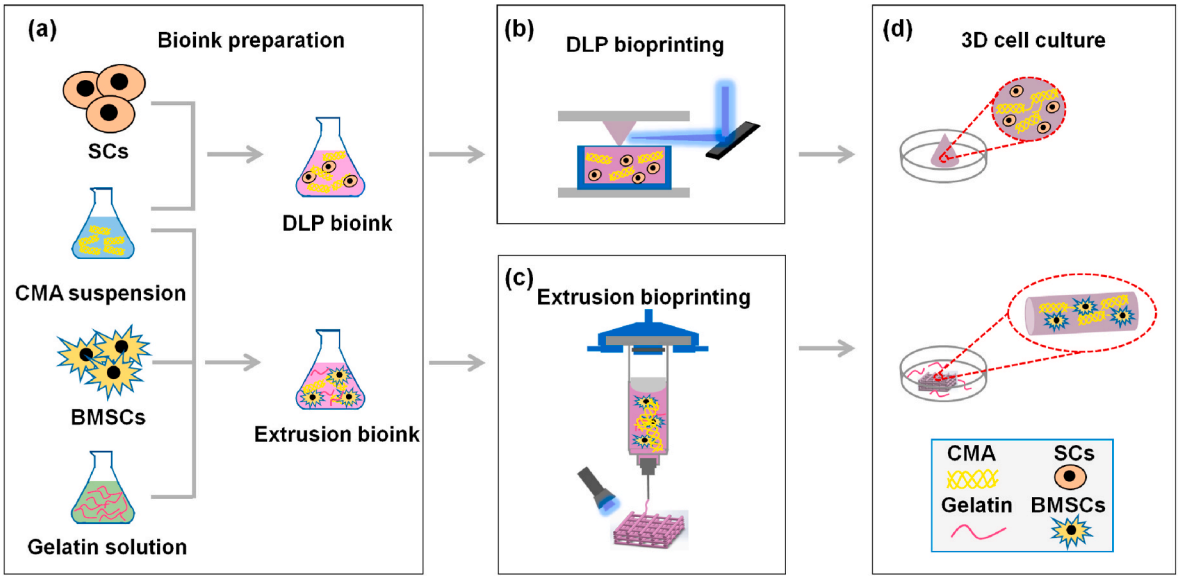

Fig. 1. Schematic showing preparation of CMA-based bioinks and 3D cell-laden bioprinting. (a) Bioink preparation of DLP and extrusion bioprinting. (b) The illustration of DLP bioprinting. (c) The illustration of extrusion bioprinting. (d) 3D cell culture after printed.

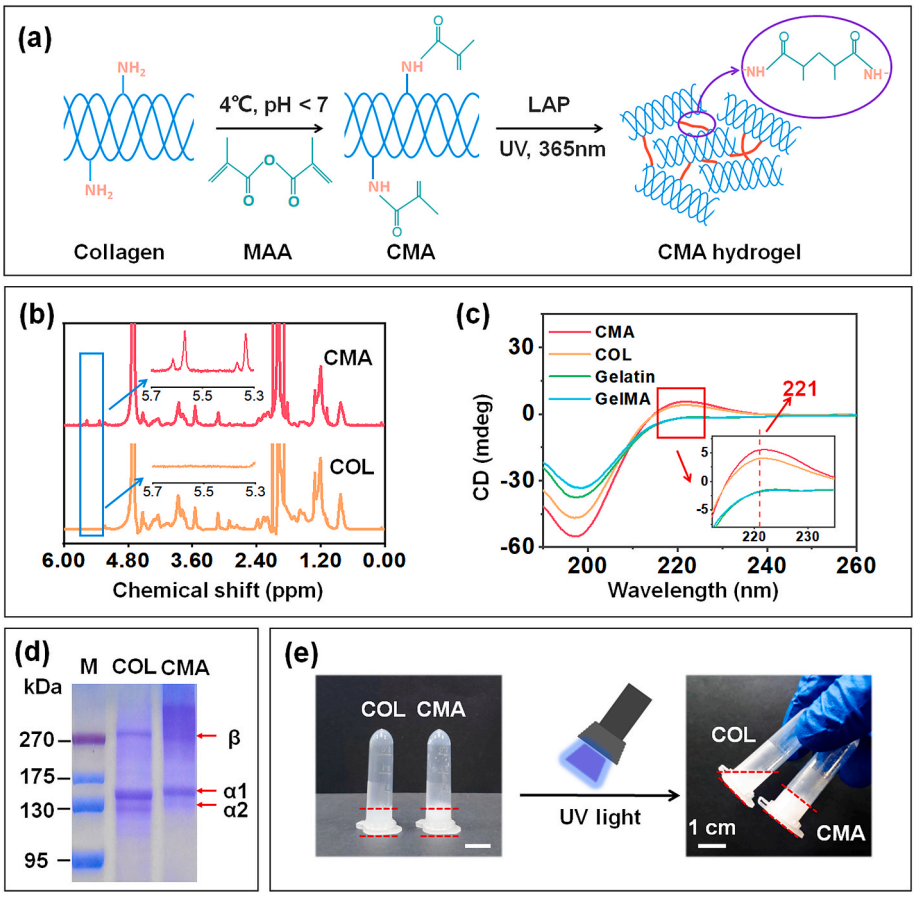

Fig. 2. Structural characterization of CMA. (a) Synthesis of CMA. (b) ^{1}H-NMR spectra of the reactant (COL) and product (CMA). (c) CD spectra of CMA, COL, gelatin, and GelMA. (d) SDS-PAGE of CMA and COL. (e) Comparison of COL and CMA after photo-crosslinking. Scale bars indicate 1 cm.

Table 1
CMA-based bioinks.

Group name	CMA (wt%)	LAP (wt%)	Gelatin (wt%)
C1.5	1.5	0.5	0
C2.0	2.0	0.5	0
C1.5G5.0	1.5	0.5	5.0
C1.5G7.5	1.5	0.5	7.5
C2.5G5.0	2.5	0.5	5.0

2.5.2. Mechanical properties

The mechanical properties were measured at 25 °C and 37 °C using a dynamic mechanical analysis instrument (ElectroForce, TA Instruments, USA). The bioinks were photo-crosslinked to form disc-shaped hydrogels with a diameter of 8 mm and thickness of 4 mm. Each sample was loaded and compressed at a displacement rate of 1 mm/min. The compressive modulus was analyzed as the slope value of the stress-strain curve in the range of 0–10%.

2.5.3. Morphology of hydrogels

Scanning electron microscopy (SEM) (SU-8010, HITACHI, Japan) was used to visualize the hydrogel network and morphology. Hydrogel samples were divided into two parts. One part was immediately frozen at −80 °C, while the other was immersed in PBS buffer, placed in a 37 °C incubator for 24 h, removed, and frozen at −80 °C. All frozen samples were then dried in a vacuum freeze-drying machine (DYYB-10, Shanghai Deyangyibang Instruments Co., Ltd., China) for 12 h. Lyophilized samples were sputtered with gold vapor for 40 s. The morphology of the hydrogels was observed. The porosity of the hydrogels was analyzed using ImageJ software (version1.8.0, National Institutes of Health, USA).

2.5.4. Swelling properties

The swelling behavior of hydrogels was assessed over 24 h in a 37 °C incubator. Hydrogel samples were immersed in PBS buffer for 24 h to reach swelling equilibrium (swelling weight, W_s). After being removed from PBS, the hydrogels were frozen, lyophilized, and weighed (dry weight, W_d). The equilibrium swelling ratio was calculated using the following formula:

$$\text{Swelling ratio} = \frac{W_s - W_d}{W_d} \times 100\% \quad (1)$$

2.5.5. Degradation properties

To assess the degradation rates, hydrogels were immersed in sterile PBS containing 2.5 U/mg collagenase type I at 37 °C. The samples were removed after 0, 4, 8, 12, and 24 h. Excess water was removed and the samples were lyophilized. The remaining mass was determined as the ratio of the lyophilized sample weight at each time point (W_r) to the initial lyophilized weight at 0 h (W_d).

$$\text{Remaining mass percentage} = \frac{W_r}{W_d} \times 100\% \quad (2)$$

2.6. 3D bioprinting

2.6.1. DLP bioprinting

The SC-laden CMA bioinks were warmed to 37 °C in the dark before DLP printing. The DLP 3D printing system [36] consisted of a UV light source (Omnicure 2000) that emitted light at 365 nm wavelength and 1.69 mW/cm^2 intensity, a digital micromirror device (DMD) that was

based on a Texas Instruments DLP module (1920 × 1080 resolution), and a z-axis mobile platform. The SC-laden CMA bioinks were deposited in the liquid tank as small droplets and were cured using UV light reflected by the DMD chip.

2.6.2. Extrusion bioprinting

A custom-made 3D extrusion bioprinting system was used in this study, as previously described [12]. The printer was driven by air pressure. The temperature of the printing head and platform was controlled by circulating water from a constant-temperature trough (DC-1006, Jiangsu Tenlin Instrument Co., Ltd., China). A UV light source (OmniCure 2000, USA) was equipped with a printer to photocrosslink the extruded 3D objects.

BMSC-laden CMA/gelatin bioinks with different CMA (1.5–3.0 wt%) and gelatin (0–10.0 wt%) ratios were prepared at 37 °C and were loaded in a 3 mL syringe. After cooling for 20 min, the CMA/gelatin bioinks were used for extrusion bioprinting. The extrudability was assessed at 20–25 °C using a nozzle with an inner diameter of 260 μm, while the extrusion pressure was set from 0.25 to 0.50 MPa. The extrudable bioink was then printed using a two-step cross-linking strategy [12]. The CMA/gelatin bioink in the syringe was maintained at 22 °C while the bioink was extruded from the nozzle and was deposited on the receiving platform. Then, the deposited 3D object was photo-crosslinked by light from a UV source (365 nm, 2–5 mW/cm^2, 2 min). The printing parameters are listed in Table 2.

2.7. Cell culture

To characterize the cytocompatibility of CMA-based hydrogels, BMSCs were embedded in different hydrogels (C1.5, C2.0, C1.5G5.0, and 10.0 wt% GelMA with ~30% methacrylation). BMSCs were cultured in α-MEM base culture medium, 10% (v/v) FBS, and 1% (v/v) P/S. The stock CMA suspension was diluted with α-MEM complete culture medium containing 0.5% LAP instead of deionized water. 10.0 wt% GelMA dissolved in α-MEM complete culture medium was used as the control group. The culture environment was maintained at 37 °C with 5% CO_2 in a humidified incubator. BMSCs were digested using 0.25% trypsin-EDTA solution when the cells reached 80% confluence. The cells were centrifuged and resuspended in CMA suspension at a final density of 1.0 × 10^6 cells/mL. Then, 100 μL BMSC-laden CMA suspension was added to a 48-well plate and photo-crosslinked under UV light (365 nm, 3 mW/cm^2) at a distance of 1 cm for 50 s at 22 °C to form CMA hydrogel embedded with BMSCs. Then, 500 μL of α-MEM complete culture medium was added to the 48-well plate. The culture medium was refreshed every two days. Cell viability and cell spreading were determined by live/dead staining after culturing for 1, 3, and 5 day. The stained hydrogels were imaged using a fluorescence microscope (Nikon Ti–U, Japan).

The designed structures with embedded SCs were DLP-printed and cultured as follows, except that SCs were cultured in DMEM complete culture medium containing 10% (v/v) FBS and 1% (v/v) P/S. The SCs-laden structures were cultured for seven days, and cell viability and morphology were observed by live/dead staining under the fluorescence microscope. SCs cultured in the CMA and GelMA hydrogels after 1, 3, 5, and 7 day were stained with DAPI and phalloidin-FITC and observed under a confocal microscope (Olympus BX61, Japan). Cell proliferation was analyzed using CCK-8 assays. Briefly, SC-laden hydrogels were placed in a 48-well plate and 400 μL DMEM complete culture medium containing 10% (v/v) CCK-8 reagent were added. The cells were cultured for 1 h. Then, 200 μL of the supernatant was aspirated into a 96-well plate and analyzed using a microplate reader (ELx800, BioTek, USA).

3D grid structures with embedded BMSCs were printed and photo-crosslinked using UV light (365 nm, 3 mW/cm^2) in extrusion bioprinting. Then, the printed grid structures containing BMSCs were transferred into a 6-well plate. 3 mL of α-MEM complete culture medium was added. The medium was refreshed every 2 days. After 7 days of culture, the BMSC viability and morphology in the printed structure were recorded by live/dead staining under the fluorescence microscope. BMSCs cultured in CMA, CMA/gelatin, and GelMA hydrogels were stained with DAPI and phalloidin-FITC and were observed using the confocal microscope. All images were analyzed using ImageJ software.

Table 2
Parameters of the extrusion printing system.

Parameter	Value
Syringe temperature (°C)	20–25
Extrusion pressure (MPa)	0.25–0.50
Cooling receiving platform temperature (°C)	15–20
XY plotting speed (mm/s)	3–5
UV light intensity (mW/cm^2)	2–5
UV exposure time after printing (min)	2
Nozzle inner diameter (μm)	260

2.8. RT-qPCR analysis

RNA from BMSCs and SCs from all samples was harvested using TRIzol (Life, MA, USA), and was dissolved in RNase-free water. The concentration and quality of the extracted RNA were measured using a Nanodrop spectrophotometer (Thermo Scientific, Waltham, MA, USA). cDNA was synthesized using FastKing gDNA Dispelling RT SuperMix kits (Tiangen, Beijing, China). Relative gene expression was analyzed using real-time PCR (Bio-Rad, Hercules, CA, USA). Power SYBR Green PCR Master Mix (Life, MA, USA) was mixed with 50 ng cDNA and specific primers (Table 3) in a total reaction volume of 10 μL.

2.9. Statistical analysis

All tests were performed at least in triplicate. Unless otherwise stated, all analyses were performed using OriginPro 2018 software (OriginLab). Statistical computations were performed using Microsoft Excel (Office 2019, Microsoft, USA). Data are expressed as mean ± standard deviation. Differences between groups were analyzed by two-way analysis of variance followed by Tukey multiple comparisons test. Significance was determined at $P < 0.05$ (*) and $P < 0.01$ (**).

3. Results

3.1. CMA synthesis

CMA in previous literature has been applied to 3D bioprinting with poor printability and a high cell death rate [32,33]. The fact that the pH of the synthesis condition was more than 7.0 [29], the temperature was room temperature [30] or the residual of organic solvent (TEA, etc) [35] had a side effect on the stability and biological properties on CMA. Therefore, to improve the printability and biocompatibility, the synthesis condition used in this study was set at 4 °C and pH was adjusted to less than 7.0. In Fig. 2b, the ^{1}H-NMR spectra of the reactant (collagen, COL) and the product (CMA) showed that the product (CMA) had absorption peaks at two positions between the chemical shifts of 5.3 and 5.7 ppm. The absorption peaks at each position appeared as spin-split doublets. In addition, the amino substitution degree of CMA was ~34.2%, as shown by BCA and TNBS experiments (Supporting Information). The CD spectra (Fig. 2c) showed that at a wavelength of 221 nm, both CMA and collagen exhibit characteristic peaks of the protein triple helix structure [35], while GelMA and gelatin did not. SDS-PAGE was also used to explore the retention of the triple-helix architecture of CMA [35]. Fig. 2d shows that CMA displayed bands corresponding to monomeric α-chains (130–170 kDa) and dimeric β-components (~270 kDa). Collagen and CMA solids were dissolved and behaved as milky-white suspensions, as shown in Fig. 2e. After UV irradiation (365 nm), the CMA suspension turned into a hydrogel, whereas the collagen

Table 3
Primer sequences.

Primer name	Sequence (F) 5′-3′	Sequence (R) 5′-3′
GAPDH	AACTCCCATTCCTCCACCTT	GAGGGCCTCTCTCTTGCTCT
SOX2	AGAACCCCAAGATGCACAAC	CTCCGGGAAGCGTGTACTTA
NANOG	GACGTGTGAAGATGAGTGAAACTGA	GTTTCCAAACAAGAA AAATCCTATGAG
OCT4	AGAGGATCACCTTGGGGTACA	CGAAGCGACAGATGGTGGTC
RUNX2	AGAGTCAGATTACAGATCCCAGG	TGGCTCTTCTTACTGAGAGAGG
ALPL	GGCTGGAGATGGACAAATTCC	CCGAGTGGTAGTCACAATGCC
COL1A1	TAAGGGTCCCCAATGGTGAGA	GGGTCCCTCGACTCCTACAT
BGP	CTGACCTCACAGATCCCAAGC	TGGTCTGATAGCTCGTCACAAG
NGF	GGACGCAGCTTTCTATCCTGG	CCCTCTGGGACATTGCTATCTG
GDNF	CTGACTTGGGTTTGGGCTAC	CCTGGCCTACCTTGTCACTT

suspension remained in a liquid state (Fig. 2e).

3.2. Cytocompatibility of CMA-based bioinks

The growth of BMSCs cultured in CMA-based hydrogels for 7 days is shown in Fig. 3a. The GelMA group (10 wt%, degree of methacrylation ~ 30%) was used as the control group. On the first day, BMSCs in CMA-based hydrogels (C1.5G5.0, C1.5, and C2.0) showed spreading, while BMSCs in the GelMA hydrogel remained spherical. On the third day, BMSCs grew vigorously in the CMA hydrogel. Further, BMSCs in the C1.5G5.0 hydrogel were connected and formed a network, while BMSCs in the GelMA hydrogel only showed slight spreading. On the fifth day, BMSCs in the C1.5G5.0 hydrogel were connected to a dense network structure and most of the BMSCs in the C1.5 and C2.0 hydrogels showed a long fusiform shape. In contrast, BMSCs in the GelMA hydrogel began to show a more obvious long fusiform shape at day 5. Cell circularity was used to characterize cell growth and spreading [37]. BMSC spreading in the CMA-based hydrogel was much better than that in the GelMA hydrogel, while BMSC spreading in CMA/gelatin was better than that in CMA hydrogels (Fig. 3c). The viability of BMSCs in both CMA and GelMA hydrogels was more than 90% (not significantly different; Fig. 3b).

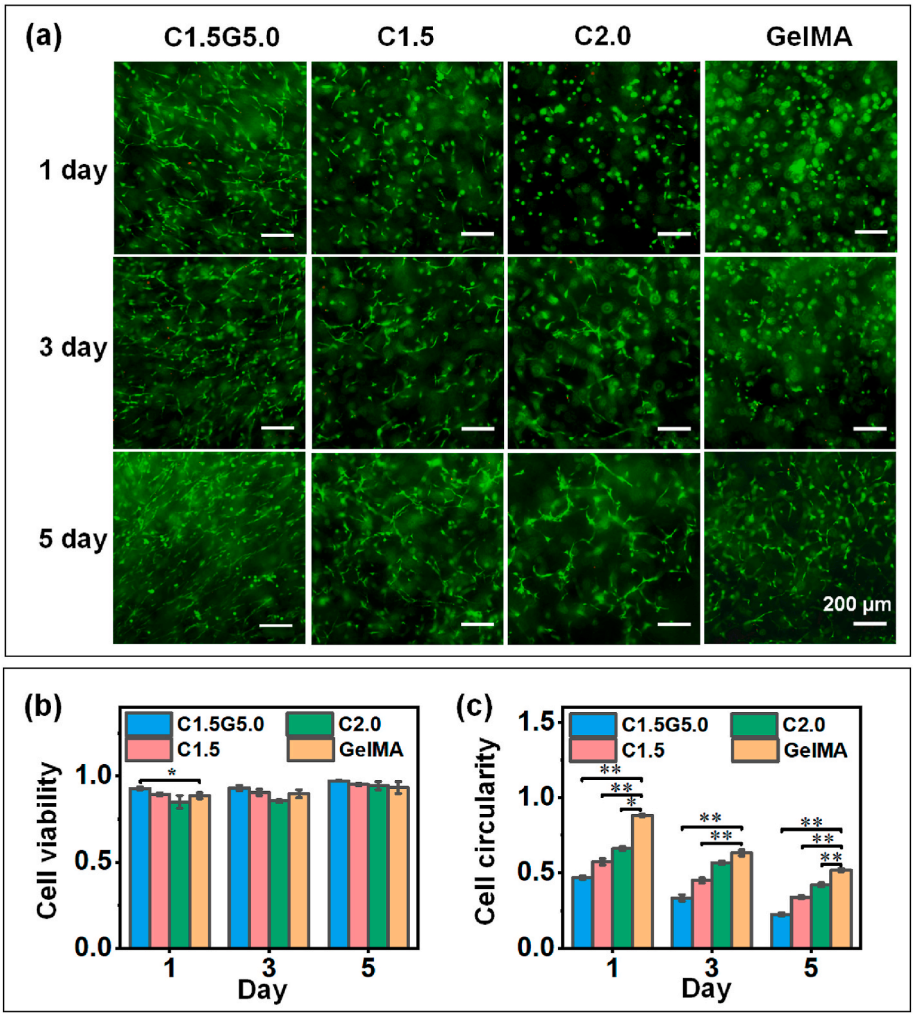

Fig. 3. (a) Fluorescence images of live/dead staining of BMSCs encapsulated in CMA-based and GelMA hydrogels on days 1, 3, and 5. Scale bars indicate 200 μm. (b) Quantification of BMSC viability (c) Quantification of cell circularity in BMSCs. C1.5G5.0: 1.5% CMA, 5.0% gelatin, and 0.5% LAP (wt). C1.5: 1.5% CMA and 0.5% LAP (wt). C2.0: 2.0% CMA and 0.5% LAP (wt). GelMA: 10.0% GelMA (wt) with ~30% methacrylation and 0.5% LAP (wt).

3.3. Rheology of CMA-based bioinks

Photo-rheological properties of the CMA bioinks significantly affected the printability of DLP bioprinting. The photorheological properties of the bioinks were determined by the different concentrations of CMA and photo-initiator (LAP) (Fig. 4a-i, Fig. 4a-ii and Fig. S2). When the LAP concentration was 0.5 wt% and the concentration of CMA increased from 1.5 wt% to 2.0 wt%, the photo-crosslinking threshold time, which is the time of the gelation point [15], gradually decreased from 16.8 s to 7.2 s. The transition modulus, which is the modulus of the gelation point, of the C1.5 bioink was the smallest. There was no obvious difference between transition moduli for the C1.75L0.5 and C2.0L0.5 bioinks (Fig. S2). When the CMA concentration was 2.0 wt% and the LAP concentration increased from 0.5 wt% to 1.0 wt%, there was no obvious difference in the threshold time and transition modulus. Considering the cytocompatibility and photo-crosslinking properties of the bioinks, the C2.0 bioink was chosen as the final DLP bioink.

Next, CMA/gelatin bioinks were used for extrusion printing as gelatin works as a regulator of CMA bioink rheology. The rheological properties of bioinks should have temperature dependence, shear thinning, shear recovery, and proper deformation resistance properties. Two bioink groups (C1.5 and C1.5G5.0) were used to illustrate the rheology of the CMA bioink with or without gelatin. Fig. 4b shows that the storage moduli (G′) and loss moduli (G″) of the bioinks are a function of temperature. At 37 °C, G′ was larger than G″, and when temperature decreased from 37 °C to 4 °C, the modulus values of the bioinks increased. The C1.5 bioink moduli increased steadily at a low rate, and there was no mutation point, whereas C1.5G5.0 bioink moduli showed an abrupt point and the temperature of mutation point of C1.5G5.0 bioink was 22.0 °C (Fig. 4b). The maximum value of G′ of C1.5G5.0 bioink was 4874.9 Pa, indicating that the gelatin in C1.5G5.0 bioink increased the modulus of bioink and improved the printability [38]. Fig. 4c shows that the viscosity of the bioink increased with decreasing temperature from 37 °C to 15 °C. The C1.5 bioink viscosity increased

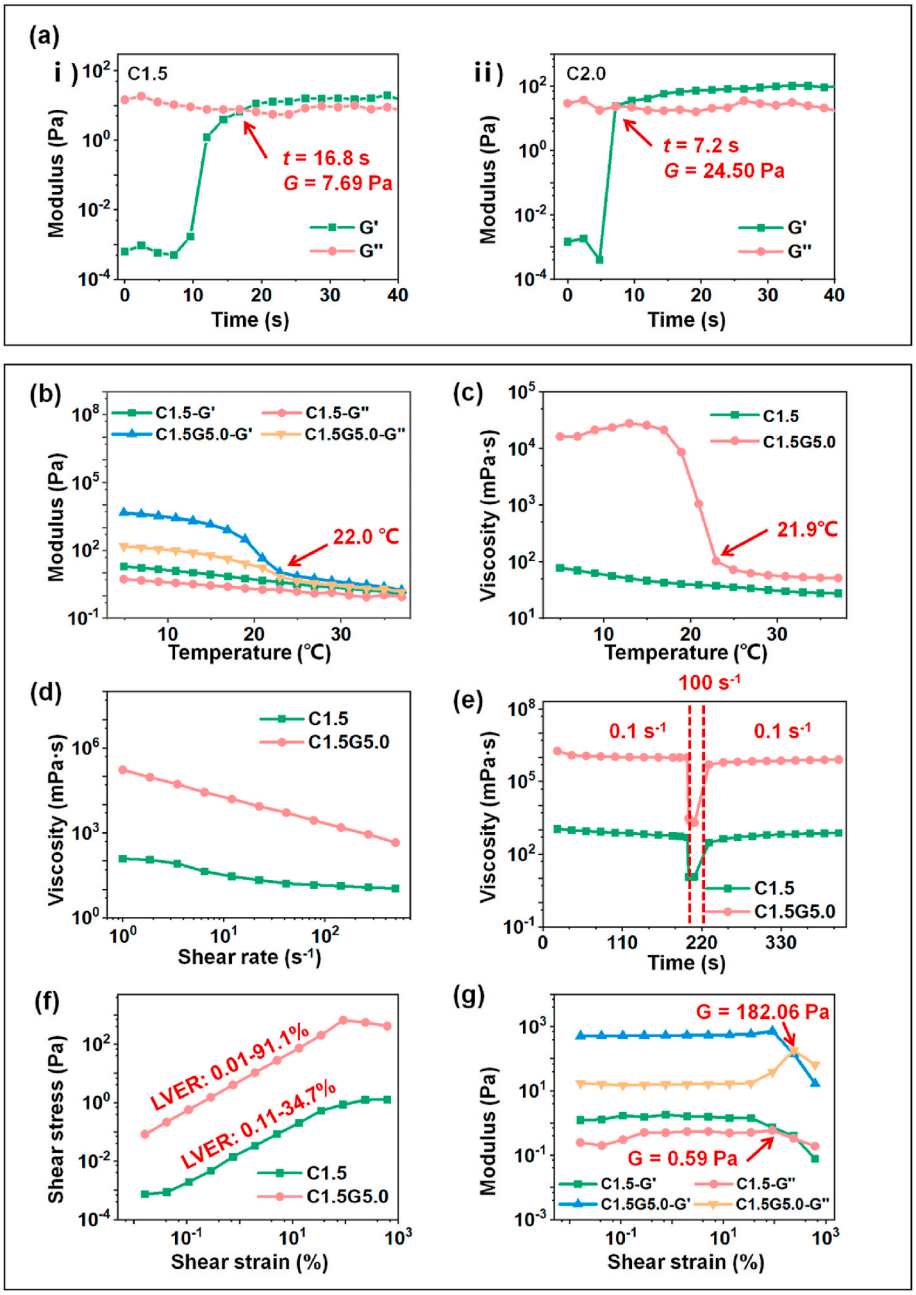

Fig. 4. Rheological properties of CMA-based bioinks. (a) (i)-(ii) Moduli of the C1.5 and C2.0 bioinks when exposed to 365 nm UV light. The red arrows represent the threshold time and transition modulus at the gelation point of the bioink. (b) Effect of temperature on the modulus of C1.5 and C1.5G5.0 bioinks. (c) Effect of temperature on the viscosity of C1.5 and C1.5G5.0 bioinks. (d) Viscosity of C1.5 and C1.5G5.0 bioinks as a function of shear rate. (e) Changes in viscosity of C1.5 and C1.5G5.0 bioinks with the application of a high shear rate. (f) Effect of shear strain on the modulus of C1.5 and C1.5G5.0 bioinks. C1.5: 1.5% CMA and 0.5% LAP (wt). C2.0: 2.0% CMA and 0.5% LAP (wt). C1.5G5.0: 1.5% CMA, 5.0% gelatin, and 0.5% LAP (wt). (For interpretation of the references to colour in this figure legend, the reader is referred to the Web version of this article.)

steadily, and the highest viscosity was 83.16 mPa s at 4 °C. The viscosity of C1.5G5.0 bioink had a sudden decrease at 21.9 °C and reached the maximum viscosity (25.66 Pa s) at 15.0 °C. C1.5G5.0 bioink exhibited a shear-thinning property, while the shear-thinning property of the C1.5 bioink was less pronounced (Fig. 4d). Fig. 4e shows the shear recovery performance of the bioink at an instantaneous high shear rate. Both C1.5 and C1.5G5.0 bioinks exhibited shear recovery properties and the viscosity of the C1.5G5.0 bioink was higher than that of the pure CMA bioink. Fig. 4f and g show the variations in stress and modulus with shear strain for the different bioinks. The linear viscoelastic region (LVER), in which G′ and G″ are constant, can be used to distinguish the structural strength of hydrogels (weak or strong). The LVER of a strong hydrogel is much broader than that of a weak hydrogel [39]. As shown in Fig. 4f, the LVER of C1.5G5.0 bioink ranged from 0.01 to 91.1%, whereas the LVER of C1.5 bioink ranged from 0.11 to 34.7%. Thus, the C1.5G5.0 bioink was stronger than the C1.5 bioink. At the crossover point (G' = G''; Fig. 4g), the modulus of the C1.5G5.0 bioink (182.06 Pa) was much larger than that of the C1.5 bioink (0.59 Pa), revealing that the C1.5G5.0 bioink better resisted deformation after printing [40]. Therefore, the addition of gelatin to the CMA bioink improved the rheological properties of the pure CMA bioink and improved the extrusion printability.

3.4. Physical properties of hydrogels

The mechanical properties of C1.5, C2.0, C1.5G5.0, GA5.0 and

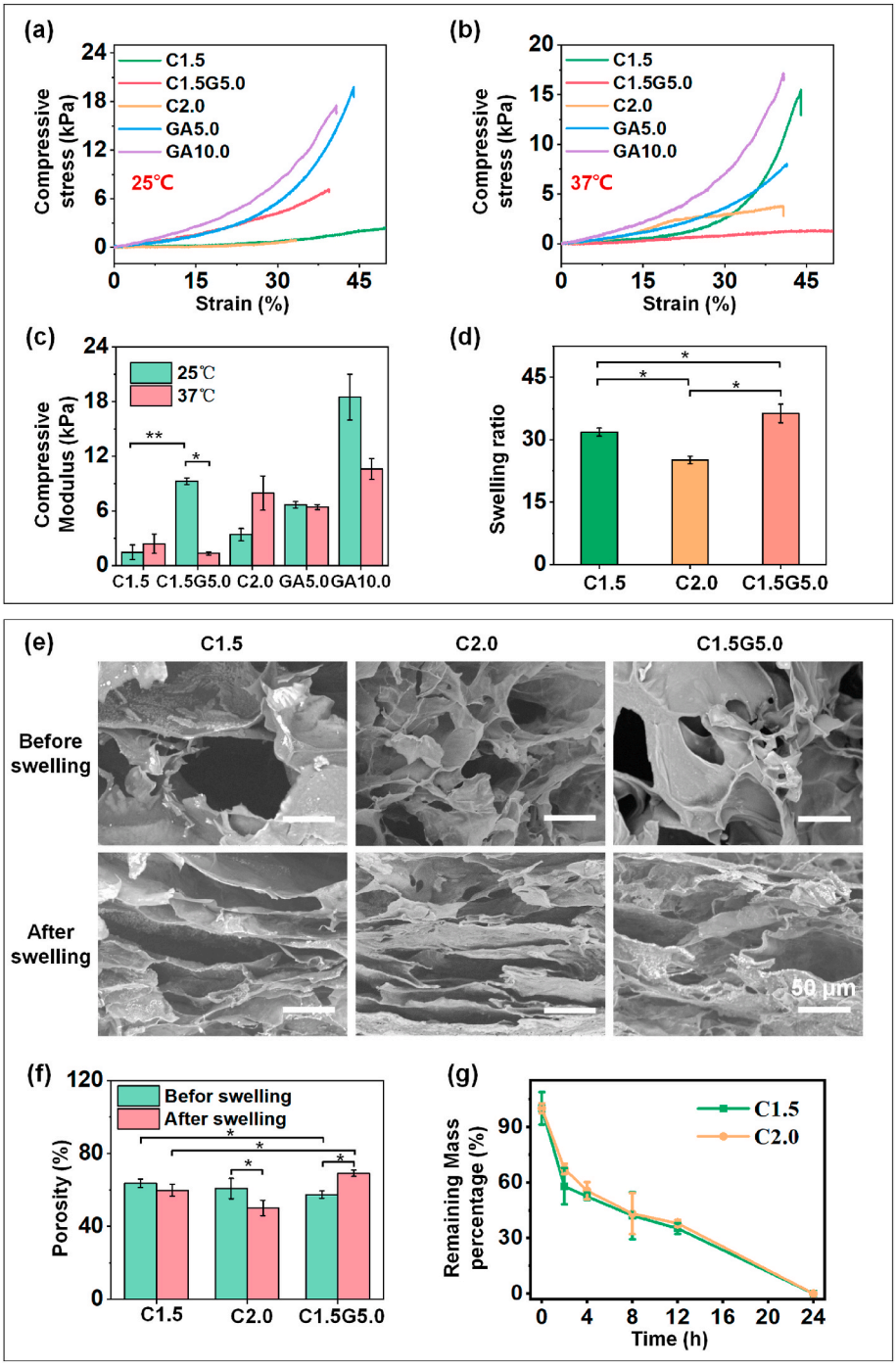

Fig. 5. Physical properties of the hydrogels. Compressive stress-strain curves of CMA-based and GelMA hydrogels at 25 °C (a) and 37 °C (b). (c) Compressive modulus of CMA-based and GelMA hydrogels at 25 °C and 37 °C. (d) Equilibrium swelling properties of CMA-based hydrogels. (g) Degradation properties of the C1.5 and C2.0 hydrogels. (d) SEM images before and after swelling at 37 °C for 24 h. The scale bars indicate 50 μm. C1.5: 1.5% CMA and 0.5% LAP (wt). C2.0: 2.0% CMA and 0.5% LAP (wt). C1.5G5.0: 1.5% CMA, 5.0% gelatin, and 0.5% LAP (wt). GA5.0: 5.0% GelMA with ~98% methacrylation and 0.5% LAP (wt). GA10.0: 10.0% GelMA and ~30% methacrylation and 0.5% LAP (wt).

GA10.0 hydrogels were tested at 25 °C and 37 °C. Fig. 5 shows the compressive stress-strain curves of hydrogels at 25 °C (a) and at 37 °C (b) and Fig. 5c shows the compressive moduli of hydrogels at different temperatures. After adding gelatin, the modulus of the C1.5G5.0 hydrogel (9.272 ± 0.365 kPa) at 25 °C was higher than that of the C1.5 hydrogel (1.469 ± 0.811 kPa). The hydrogel modulus increased slightly to 3.395 ± 0.667 kPa when the CMA concentration increased to 2.0 wt %. The moduli of the C1.5 (2.406 ± 1.062 kPa) and C2.0 (7.969 ± 1.880 kPa) hydrogels at 37 °C were higher than those at 25 °C because CMA hydrogels would shrink [41]. The modulus of C1.5G5.0 (1.337 ± 0.180 kPa) hydrogels at 37 °C were lower than those at 25 °C because the gelatin was released at a high temperature. For GelMA hydrogels, the modulus of GA 5.0 at 25 °C (6.681 ± 0.356 kPa) was a little higher than the value at 37 °C (6.428 ± 0.267 kPa); the modulus of GA10.0 at 25 °C (18.492 ± 2.490 kPa) was much higher than the value at 37 °C (10.585 ± 1.142 kPa). The moduli of C2.0 and GA5.0 hydrogels were approximately equal at 37 °C.

The swelling behaviors of the C1.5, C2.0, and C1.5G5.0 hydrogels are presented in Fig. 5d.The swelling ratio of the C2.0 hydrogel (36.325 ± 2.758) was larger than that of C1.5 hydrogel (31.813 ± 1.253). For the C1.5G5.0 hydrogel (25.126 ± 1.095), the addition of gelatin reduced the swelling ratio of the CMA hydrogel because the gelatin was partly dissolved and some gelatin was entangled by the CMA network, leading to a lower swelling ratio [12]. Fig. 5e presents the morphologies of C1.5, C2.0, and C1.5G5.0 hydrogels before and after swelling at 37 °C for 24 h. Before swelling, the interiors of hydrogels were mostly circular pore structures and the porosity (Fig. 5f) of the C1.5 hydrogel (63.637 ± 2.486%) was the largest. After swelling, the porosity of the C1.5 hydrogel (59.875 ± 3.219%) decreased, while the porosity of the C1.5G5.0 hydrogel increased to 69.115 ± 1.727%.As shown in Fig. 5g, enzymatic degradation experiments showed that both the C1.5 and C2.0 hydrogels were completely degraded within 24 h.

3.5. Printability of CMA-based bioinks

3.5.1. DLP bioprinting

A quadrangular pyramid with a base length and height of 5 mm was designed to demonstrate DLP bioprinting (Fig. 6a-i). C2.0 bioink and 5% GelMA (~98% methacrylation) were printed. Microscope photos of the cross-section of printed structures before and after freeze-drying (Fig. 6a-ii, iii, v and vi) were used to characterize the boundary roughness. The roughness of the printed pyramid surface before freeze-drying is indicated by the arithmetic mean deviation (R_a), which was calculated as follows:

$$R_a = \frac{1}{l}\int_0^l |z(x)|dx \tag{3}$$

where l is the basic length of the printed structure and $z(x)$ is the normal distance between the actual structure and the design model. As shown in Fig. 6a-ii and iii, the R_a of structure printed using GelMA bioink was 38.66 ± 19.76 and the R_a of structure printed by CMA bioink was 16.32 ± 7.43. This result indicates that CMA bioink has a better shape fidelity than GelMA bioink. Fig. 6b shows DLP-printed structures using the CMA bioink. Multichannel hollow circular tubes (Fig. 6b-i and ii) and quadrangular pyramids (Fig. 6b-iii and iv) were successfully printed.

3.5.2. Extrusion bioprinting

Bioinks with different CMA/gelatin concentration ratios were extruded using the printing parameters listed in Table 2 to obtain bioinks that could be continuously and stably extruded into filaments. Three composite bioink groups (C1.5G5.0, C2.5G5.0, and C1.5G7.5) were selected from the blue region in Fig. S3 to illustrate extrusion printability.

Isometric grids with 1-mm intervals were designed to test the bioink printability. The bioink printability was defined as follows [42]:

$$\mathrm{Pr} = \frac{L^2}{16A} \tag{4}$$

where, L means perimeter and A mean area. For ideal printability, the interconnected channels of the constructs would demonstrate square shape, and the value of Pr is 1. As shown in Fig. 7a and c, and Fig. S4a, the Pr of grids printed with C1.5G5.0 bioink (blue) was closer to 1.0, while the Pr values of grids printed with C2.5G5.0 (yellow) or C1.5G7.5 bioink (red) were 1.45 ± 0.13 and 0.84 ± 0.03, respectively. A filament collapse test was also performed, in which the mid-span deflection of suspended bioink filaments was assessed [43]. Printing a filament across gaps of increasing distance can measure the deflection of the filament and quantify the shape fidelity [44]. In this study, the receiver substrate (Fig. S4a) was designed to characterize the degree of collapse of the extruded microfilaments. The degree of collapse was indicated by the collapse area factor:

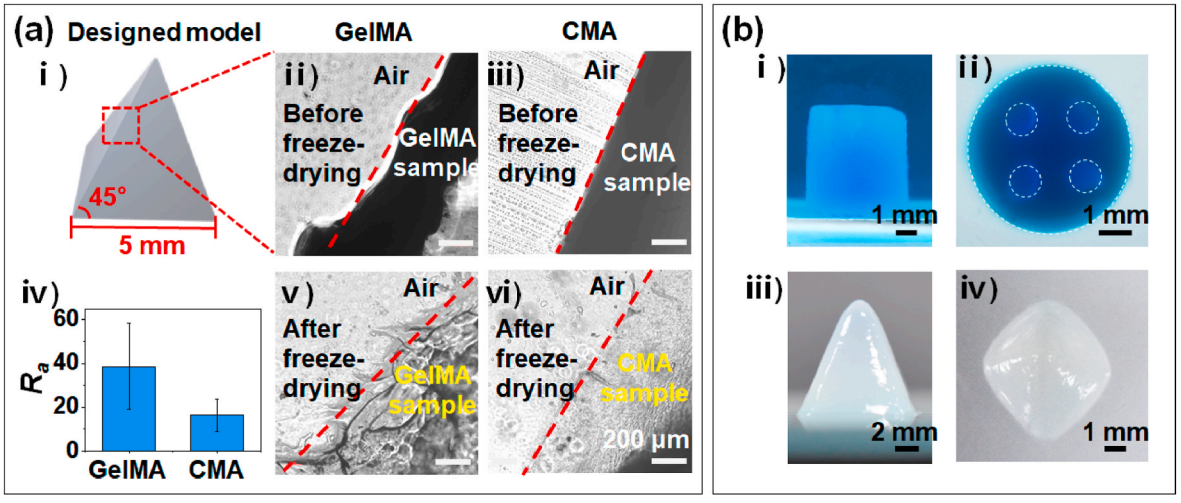

Fig. 6. DLP printability of the CMA bioink. (a) i) designed model. ii) The microscope photo of the cross-section of the structure printed by GelMA bioink before freeze-drying. iii) Microscope photo of the cross-section of the structure printed by CMA bioink before freeze-drying. iv) R_a values calculated from structures printed with CMA and GelMA bioinks. v) The microscope photo of the cross-section of the structure printed by GelMA bioink after freeze-drying. vi) Microscope photo of the cross-section of the structure printed by CMA bioink after freeze-drying. Scale bars indicate 200 μm. (b) Structures printed using CMA bioink. (i, ii) Multichannel hollow circular tubes. (iii, iv) triangular pyramids. CMA: C2.0 (2.0% CMA and 0.5% LAP (wt)). GelMA: 5.0% GelMA (wt) with ~98% methacrylation.

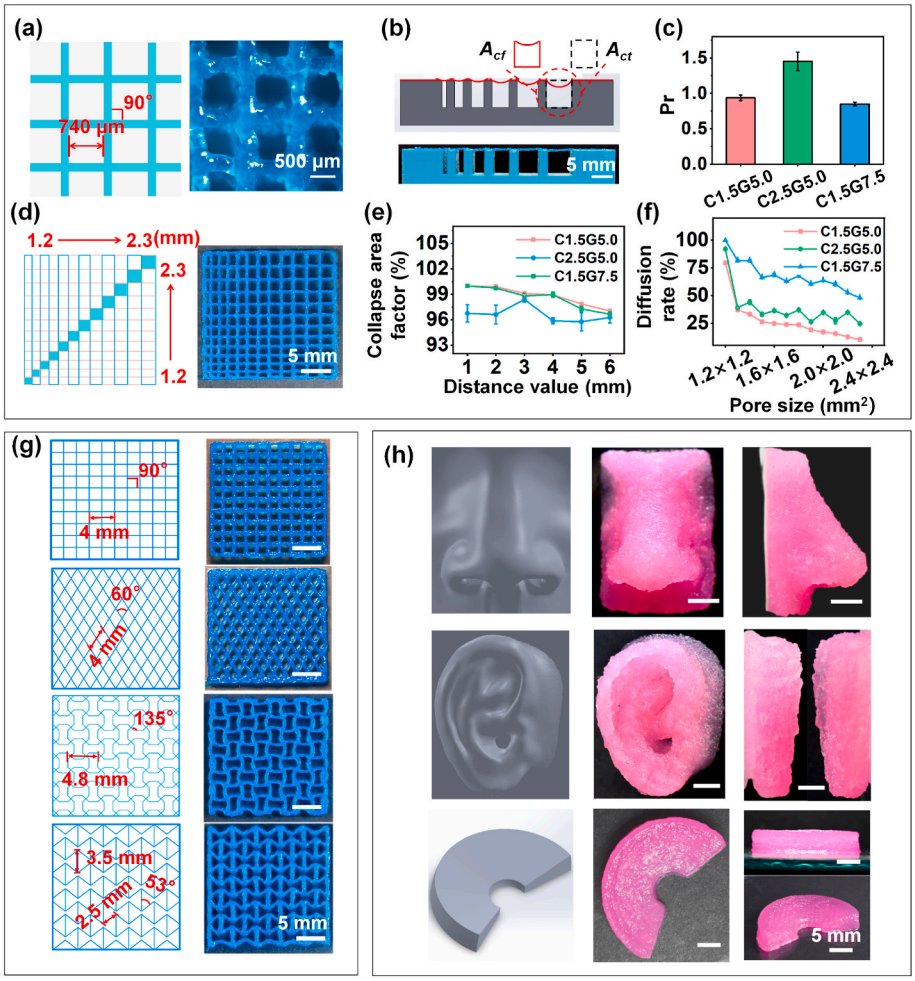

Fig. 7. Extrusion printability characterization of the CMA/gelatin composite bioinks. (a) Shape fidelity test of a grid structure printed using C1.5G5.0 bioink. Scale bars indicate 500 μm. (b) Filament collapse test of C1.5G5.0 bioink. Scale bars indicate 5 mm. (c) Pr values calculated from the structures printed with C1.5G5.0, C2.5G5.0, and C1.5G7.5 bioinks. (d) Filament diffusion test of C1.5G5.0 bioink. Scale bars indicate 5 mm. (e) Quantitative analysis of filament collapse tests using C1.5G5.0, C2.5G5.0, and C1.5G7.5 bioinks. (f) Quantitative analysis of filament diffusion tests using C1.5G5.0, C2.5G5.0, and C1.5G7.5 bioinks. (g) 2D graphics (grid, diamond, and negative Poisson's ratio structures) printed using C1.5G5.0 bioink. Scale bars indicate 5 mm. (f) 3D objects (human nose, ear, and meniscus) printed using C1.5G5.0 bioink. Scale bars indicate 5 mm. C1.5G5.0:1.5% CMA, 5.0% gelatin, and 0.5% LAP (wt). C2.5G5.0: 2.5% CMA, 5.0% gelatin, and 0.5% LAP (wt). C1.5G7.5: 1.5% CMA, 7.5% gelatin, and 0.5% LAP (wt).

$$\text{Collapse area factor} = \frac{A_{cf}}{A_{ct}} \times 100\% \quad (5)$$

where A_{cf} and A_{ct} are as shown in Fig. 7b. The filament (blue, Fig. 7b) extruded using the C1.5G5.0 bioink had the lowest collapse (Fig. 7e), whereas the filaments extruded by the C2.5G5.0 bioink (yellow, Fig. S4b), and C1.5G7.5 bioink (red, Fig. S4b) showed similar collapse. Moreover, designed unequal grids whose grid intervals were expanded from 1.2 mm to 2.3 mm in 0.1-mm steps were printed with the bioinks. The percentage deviation of the printed diagonal squares of the actual grid area (A_{df}) from the theoretical square area (A_{dt}) was defined as the diffusion rate.

$$\text{Diffusion rate} = \frac{(A_{dt} - A_{df})}{A_{dt}} \times 100\% \quad (6)$$

Fig. 7d and f, and Fig. S4c shows that, under the designed printing path, graphics (blue, Fig. 7d) printed with the C1.5G5.0 bioink had the lowest diffusion rate and a relatively stable diffusion rate, while graphics printed with the C2.5G5.0 bioink (yellow, Fig. S4c) and C1.5G7.5 bioink (red, Fig. S4c) had a higher diffusion rate and less stable variation.

Based on the characterization of the printability of CMA/gelatin bioinks with different concentration ratios, C1.5G5.0 bioink was determined to be the best choice for extrusion bioprinting. As shown in Fig. 7g and h, 2D graphics (square mesh, diamond mesh, and two negative Poisson's ratio structures) and 3D objects (human nose, ear, and meniscus) were printed using the bioink.

3.6. Cell bioprinting and culturing in CMA-based hydrogels

Heart, pentagram, and crescent shapes were DLP bioprinted with C2.0 bioink or GelMA (5 wt%, ~98% methacrylation) bioink and embedded with SCs. After 5 days of culture, SCs grew and were distributed evenly in the CMA hydrogel. In contrast, the SCs grew in clumps in the GelMA hydrogel (Fig. 8a). Furthermore, confocal 3D imaging (Fig. 8b and Fig. S7) showed that after 7 culture days, SC processes outgrowth was observed within the CMA hydrogel, whereas SCs in the GelMA hydrogel remained spherical. Furthermore, Fig. 8c shows that SCs had higher proliferation in the CMA hydrogel than in the GelMA hydrogel. The expression of neurotrophic factors, including GDNF and NGF, was evaluated in SCs cultured in C2.0- and GelMA bioinks after 6 days (Fig. 8d). SCs grown in GelMA and CMA hydrogels had similar GDNF gene expression (1.11- and 1.12-fold, respectively; normalized to 2D culture). However, NGF gene expression was significantly upregulated in the CMA sample compared to the GelMA sample.

The C1.5G5.0 bioink with BMSCs was printed by extrusion. The BMSCs grew and spread well after 1, 3, and 5 days of culture (Fig. 9a). Fig. 9b shows the 3D morphology of BMSCs inside the three hydrogels (CMA/gelatin, CMA, and GelMA). The BMSCs were encapsulated in CMA/gelatin and CMA hydrogels and were distributed within a tight network. To compare the morphology of BMSCs spreading in different bioinks, a 400 μm-thick layer near the surface of the hydrogels was chosen for confocal 3D observation of the cytoskeleton and nucleus area ratio of the BMSCs. As shown in Fig. 9c, BMSCs in GelMA grew inconsistently and only spread normally within 120 μm near the surface. BMSCs in CMA/gelatin and CMA spread better than those laden in

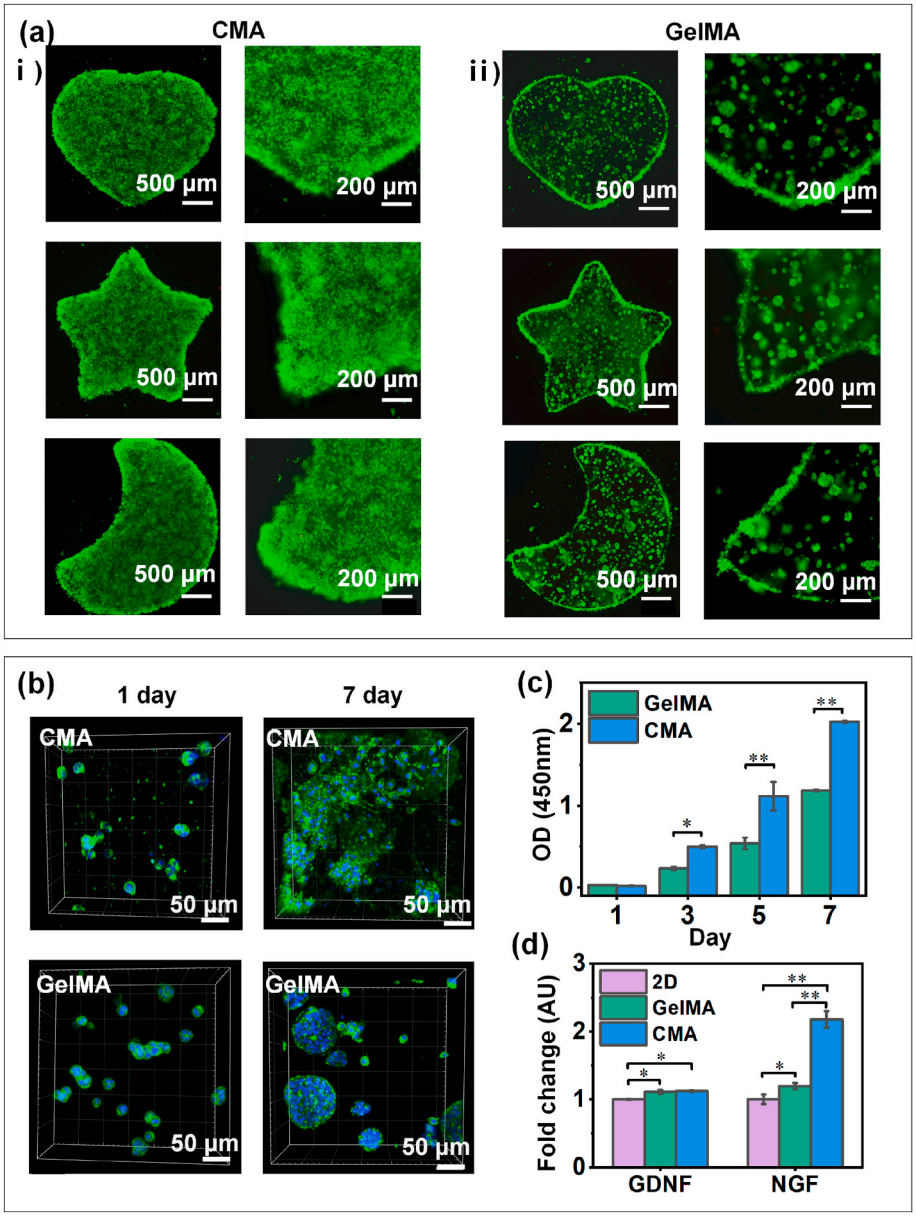

Fig. 8. DLP bioprinting and SC culture in hydrogels. (a) Heart, pentagram, and crescent structures were bioprinted by DLP using CMA and GelMA bioinks containing SCs. The embedded cells were cultured for five days. (b) Confocal 3D images of SC-laden hydrogels after culturing for seven days. (c) Quantification of SC proliferation in different hydrogels on days 1, 3, 5, and 7 using CCK-8 assays. (d) RT-qPCR analysis of SCs grown on a petri dish (2D) and in hydrogels. CMA: C2.0 (2.0% CMA and 0.5% LAP (wt)). GelMA: 5 wt% and ~98% methacrylation.

GelMA with BMSCs spreading consistently on the printed surface or within the printed shape.

The expression of the stemness markers SOX2, NANOG, and OCT4 was evaluated by RT-qPCR for BMSCs after culturing for 6 days (Fig. 9d and e). All samples showed upregulated stemness gene expression compared to cells in 2D culture. CMA/gelatin and CMA samples had significantly higher SOX2 expression compared to GelMA, with 8.46-, 11.14-, and 13.98-fold higher expression, respectively (normalized to 2D culture). However, the expression of NANOG and OCT4 in CMA/gelatin and CMA samples was significantly downregulated compared with the GelMA sample. RUNX2, ALPL, COL1A1, and BGP gene expression was further analyzed to evaluate the osteogenic differentiation of BMSCs. CMA samples had 7.95-, 19.07-, 12.66-, and 30.04-fold expression, respectively (normalized to 2D culture). And the NANOG, OCT4, COL1A1, RUNX2, and Osteocalcin protein expression of BMSCs were analyzed with immunofluorescence staining (Fig. S8), which demonstrates similar results with RT-qPCR.

4. Discussion

GelMA, containing arginine-glycine-aspartic acid (RGD) sequences that promote cell adhesion has been extensively used in 3D bioprinting for its good biocompatibility. However, it loses the unique triple-helix molecular structure of collagen [19] because gelatin was thermal denaturation products of collagen. According to previous studies, the unique triple-helix molecular structure of collagen containing the polypeptide sequence Gly–Pro–Hyp (GPO) [21] and Gly Phe-Hyp (GFO) [22] motifs, would activate signals and facilitate communication between cells. For example, the widely expressed mammalian discoidin domain receptors (DDRs), DDR1 and DDR2, as receptor protein tyrosine kinases that facilitate cellular functions include cell migration, cell survival, proliferation and remodeling of extracellular matrices [45], are activated by the extracellular matrix collagen [46].

Collagen bioink is rarely printed directly in 3D printing due to its poor printability, leading to the development of CMA to improve the crosslinking degree and gelation rate for 3D printing. Several studies have synthesized CMA and prepared CMA-based bioink, but still limited by the low printability and high cellular death rate [32,33], so CMA was

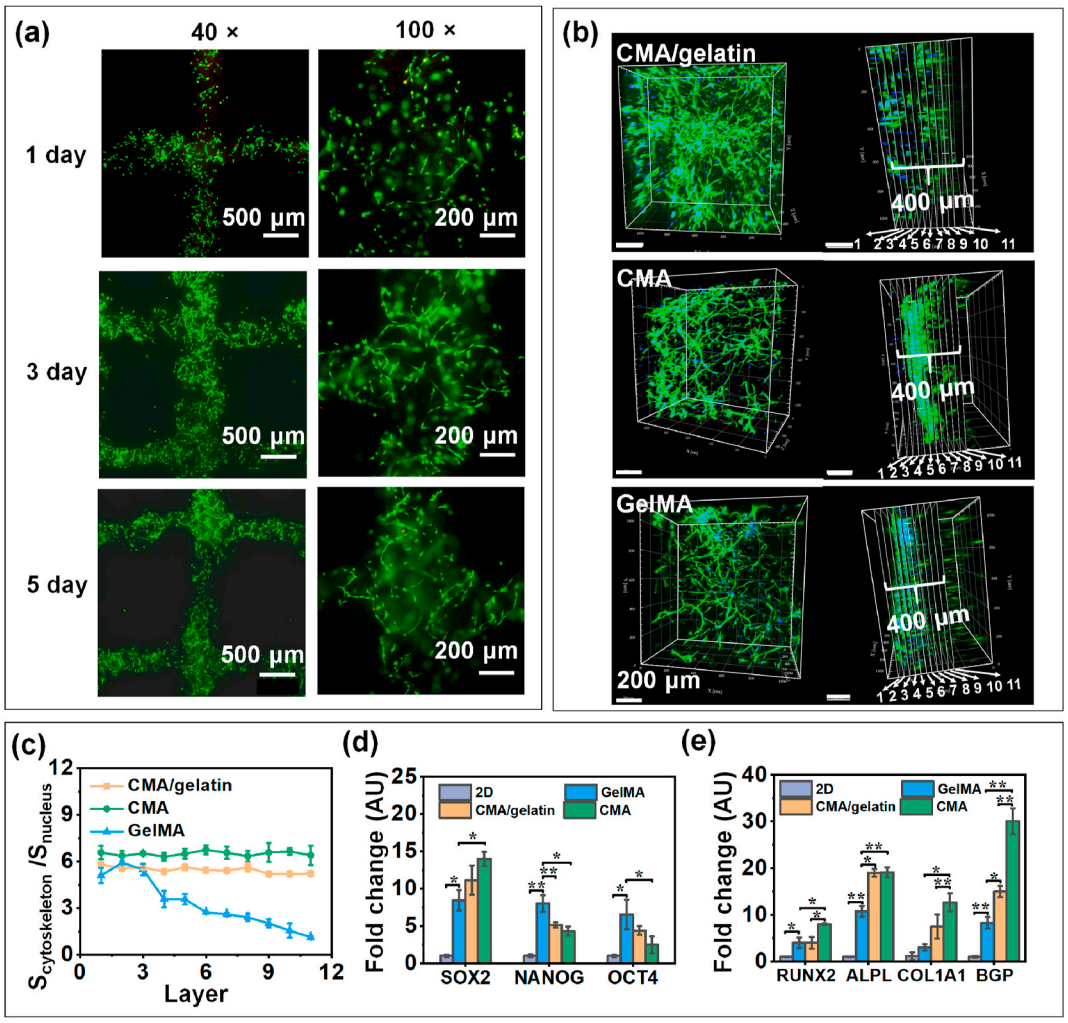

Fig. 9. Extrusion bioprinting and BMSC culture in hydrogels. (a) Grid structures were bioprinted using CMA/gelatin bioink containing BMSCs. The cells in the printed grids were cultured for 1, 3, and 5 d. (b) Confocal 3D images of BMSC-laden hydrogels after culturing for 7 days. (c) Quantitative analysis of the ratio between the cytoskeleton and nucleus areas of BMSCs grown in different hydrogels and layers. (d, e) RT-qPCR analysis of BMSCs grown in a Petri dish (2D) and loaded into hydrogels. CMA/gelatin: C1.5G5.0 (1.5% CMA, 5.0% gelatin, and 0.5% LAP (wt.)). CMA: C1.5 (1.5% CMA and 0.5% LAP (wt)). GelMA: 10 wt% and ~30% methacrylation.

not widely used in 3D printing for tissue engineering. Here, we modified the synthetic conditions of CMA with 4 °C and pH < 7.0 to obtain a high cell viability in CMA hydrogels (>90%). For printability, the efficiency of DLP bioprinting could be effectively regulated (Fig. 4a and Fig. S2) by adjusting the concentration of CMA and photoinitiator (LAP). Compared to GelMA bioink, the constructs printed by CMA bioink have smoother surfaces.

The CMA bioink itself has a low storage modulus before extrusion [38], while adding gelatin to CMA bioink can regulate the rheology of CMA/gelatin bioink (Fig. 4b). Therefore, CMA/gelatin bioink can be applied for extrusion bioprinting. 3D complex organs or tissue structure including nose, ear and meniscus are obtained by CMA/gelatin bioink which has similar printability with GelMA bioink. After printing, the methylacrylamide groups in CMA are irreversibly photo-crosslinked, while gelatin dissolved at 37 °C.

BMSCs and SCs were printed using extrusion and DLP to analyze the biological properties of CMA under various conditions. Both cells demonstrated the cellular viability higher than 90% after 7 days of culture, which was much better than the CMA developed in other studies [32,33]. During the culture, SCs exhibited process outgrowth within structures printed with CMA, while SCs remained spherical in GelMA (Fig. 8a and b, and Fig. S7). In addition, SCs encapsulated in CMA had a higher proliferation rate than those in the GelMA sample (Fig. 8c). The expression of neural stem cell-associated genes for SCs cultured in CMA was significantly higher culture compared to that in GelMA (Fig. 8d), indicating that SCs could better support the growth of neural stem cells. Considering that the stiffness of hydrogels influences the glial cells [47], here we chose approximately equal elastic modulus of GelMA and CMA hydrogels at 37 °C (Fig. 5c) to culture SCs to exclude the influence of stiffness, and we made the preliminary conclusion that the unique triple-helix molecular structure of CMA was the reason of the biological results [48–50].

BMSCs encapsulated in CMA-based hydrogels showed better cell spreading (Figs. 3, 9b and 9c) and expressed more osteogenesis-related genes than the GelMA sample, suggesting that CMA-based hydrogels could induce osteogenic differentiation of BMSCs without the addition of an osteogenic differentiation inducer [51]. A recent study has illustrated that the matrix stiffness is an important cue for regulating the differentiation of BMSCs, and soft matrices limit the osteogenic differentiation, therefore BMSCs in CMA had higher osteogenesis-related gene expression than CMA/gelatin hydrogels, since CMA was relatively stiffer [52]. Comparing the moduli of CMA and CMA/gelatin hydrogels at 37 °C (Fig. 5c), because the CMA/gelatin group is softer than CMA group, Fig. 9e shows that BMSCs expression more osteogenesis-related genes than CMA sample. Moreover, BMSCs with high cell spreading inside the CMA would have better cell-cell and cell-extracellular matrix

interactions, which could be caused by the CMA with typical triple-helix α-peptide chains assists intercellular signal transmission and functional expression. Previous study demonstrated that keratinocytes cultured on collagen had higher adhesion and proliferation rates than those cultured on gelatin or collagen hydrolysates [53]. Our results indicate that cells cultured within CMA have better physiological effects than those cultured in GelMA. A previous study indicated that 7 mg/mL collagen hydrogels loaded with different densities of BMSCs cultured for 28 days had different differentiation results [51]. Our study had a slightly different experimental setup. Next, we will adjust the experimental setup to induce BMSCs to differentiate into other functional cells, such as chondrocytes and adipocytes. Overall, we concluded that CMA is a promising biomaterial in 3D bioprinting.

5. Conclusion

In this study, we investigated the printability of CMA-based bioink and compared the effects of CMA and GelMA-based bioink on the cells encapsulated in the printed constructs. For poor printability of collagen, we synthesized the photocurable biomaterial CMA and prepared SCs-laden bioinks for DLP bioprinting. In addition, a gelatin pre-crosslinking mechanism was introduced to prepare CMA/gelatin composite bioink, thereby realizing the application of collagen in extrusion bioprinting. The cell viability, spreading, proliferation, and gene expression of the encapsulated cells were evaluated and found that CMA has better effects on cellular behavior compared with GelMA, and DLP can print high fidelity structures with more smooth surfaces using CMA bioink than GelMA bioink. Also, the insolubility of CMA in water influences its manipulation and the poor mechanical properties limit its application in 3D bioprinting. But we would like to overcome the shortcomings in our next work. In conclusion, the CMA developed in this study has immense potential for tissue engineering and regenerative medicine applications in the future.

Credit author statement

Huimin Shi: methodology, software, validation, formal analysis, writing-original draft. Yang Li: methodology, formal analysis, writing-original draft. Kailei Xu: methodology, writing-review & editing. Jun Yin: conceptualization, writing-review & editing, funding acquisition, supervision.

Declaration of competing interest

The authors declared no potential conflicts of interest with respect to the research, authorship, and/or publication of this article.

Data availability

Data will be made available on request.

Acknowledgements

The authors gratefully acknowledge the support provided by the National Natural Science Foundation of China (Nos. 52250006 and 52075482) and the Starry Night Science Fund of Zhejiang University Shanghai Institute for Advanced Study (No. SN-ZJU-SIAS-004).

Appendix A. Supplementary data

Supplementary data to this article can be found online at https://doi.org/10.1016/j.mtbio.2023.100799.

References

[1] C. Luan, P. Liu, R. Chen, B. Chen, Hydrogel based 3D carriers in the application of stem cell therapy by direct injection, Nanotechnol. Rev. 6 (5) (2017) 435–448.
[2] D. Hou, E.A.-S. Youssef, T.J. Brinton, P. Zhang, P. Rogers, E.T. Price, A.C. Yeung, B. H. Johnstone, P.G. Yock, K.L. March, Radiolabeled cell distribution after intramyocardial, intracoronary, and interstitial retrograde coronary venous delivery, Circulation 112 (9_supplement) (2005). I-150-I-156.
[3] R. Langer, J.P. Vacanti, Tissue engineering, Science 260 (5110) (1993) 920–926.
[4] Q. Mao, Y. Wang, Y. Li, S. Juengpanich, W. Li, M. Chen, J. Yin, J. Fu, X. Cai, Fabrication of liver microtissue with liver decellularized extracellular matrix (dECM) bioink by digital light processing (DLP) bioprinting, Mater. Sci. Eng. C 109 (2020), 110625.
[5] J. Yan, X. Liu, J. Liu, X. Zhang, Q. Zheng, J. Nan, M. Lin, H. Pan, Y. Wang, X. Cai, J. Yin, A dual-layer cell-laden tubular scaffold for bile duct regeneration, Mater. Des. 212 (2021), 110229.
[6] A. Lee, A.R. Hudson, D.J. Shiwarski, J.W. Tashman, T.J. Hinton, S. Yerneni, J. M. Bliley, P.G. Campbell, A.W. Feinberg, 3D bioprinting of collagen to rebuild components of the human heart, Science 365 (6452) (2019) 482–487.
[7] P. Bajaj, R.M. Schweller, A. Khademhosseini, J.L. West, R. Bashir, 3D biofabrication strategies for tissue engineering and regenerative medicine, Annu. Rev. Biomed. Eng. 16 (1) (2014) 247–276.
[8] D.J. Mooney, D.F. Baldwin, N.P. Suh, J.P. Vacanti, R. Langer, Novel approach to fabricate porous sponges of poly(d,l-lactic-co-glycolic acid) without the use of organic solvents, Biomaterials 17 (14) (1996) 1417–1422.
[9] D. Zhao, H. Zhou, Y. Wang, J. Yin, Y. Huang, Drop-on-demand (DOD) inkjet dynamics of printing viscoelastic conductive ink, Addit. Manuf. 48 (2021), 102451.
[10] T. Xu, W. Zhao, J.-M. Zhu, M.Z. Albanna, J.J. Yoo, A. Atala, Complex heterogeneous tissue constructs containing multiple cell types prepared by inkjet printing technology, Biomaterials 34 (1) (2013) 130–139.
[11] J. Liu, B. Zhang, L. Li, J. Yin, J. Fu, Additive-lathe 3D bioprinting of bilayered nerve conduits incorporated with supportive cells, Bioact. Mater. 6 (1) (2021) 219–229.
[12] J. Yin, M. Yan, Y. Wang, J. Fu, H. Suo, 3D bioprinting of low-concentration cell-laden gelatin methacrylate (GelMA) bioinks with a two-step cross-linking strategy, ACS Appl. Mater. Interfaces 10 (8) (2018) 6849–6857.
[13] R. Gauvin, Y.-C. Chen, J.W. Lee, P. Soman, P. Zorlutuna, J.W. Nichol, H. Bae, S. Chen, A. Khademhosseini, Microfabrication of complex porous tissue engineering scaffolds using 3D projection stereolithography, Biomaterials 33 (15) (2012) 3824–3834.
[14] M. Gou, X. Qu, W. Zhu, M. Xiang, J. Yang, K. Zhang, Y. Wei, S. Chen, Bio-inspired detoxification using 3D-printed hydrogel nanocomposites, Nat. Commun. 5 (1) (2014) 3774.
[15] Y. Li, Q. Mao, X. Li, J. Yin, Y. Wang, J. Fu, Y. Huang, High-fidelity and high-efficiency additive manufacturing using tunable pre-curing digital light processing, Addit. Manuf. 30 (2019), 100889.
[16] M. Hospodiuk, M. Dey, D. Sosnoski, I.T. Ozbolat, The bioink: a comprehensive review on bioprintable materials, Biotechnol. Adv. 35 (2) (2017) 217–239.
[17] X. Liu, J. Yan, J. Liu, Y. Wang, J. Yin, J. Fu, Fabrication of a dual-layer cell-laden tubular scaffold for nerve regeneration and bile duct reconstruction, Biofabrication 13 (3) (2021), 035038.
[18] R. Magazine, B. van Bochove, S. Borandeh, J. Seppälä, 3D inkjet-printing of photo-crosslinkable resins for microlens fabrication, Addit. Manuf. 50 (2022), 102534.
[19] M.C. Echave, P. Sánchez, J.L. Pedraz, G. Orive, Progress of gelatin-based 3D approaches for bone regeneration, J. Drug Deliv. Sci. Technol. 42 (2017) 63–74.
[20] J.M. Lee, S.K.Q. Suen, W.L. Ng, W.C. Ma, W.Y. Yeong, Bioprinting of collagen: considerations, potentials, and applications, Macromol. Biosci. 21 (1) (2021), 2000280.
[21] P.A. Smethurst, D.J. Onley, G.E. Jarvis, M.N. O'Connor, C.G. Knight, A.B. Herr, W. H. Ouwehand, R.W. Farndale, Structural basis for the platelet-collagen interaction: the smallest motif within collagen that recognizes and activates platelet glycoprotein VI contains two glycine-proline-hydroxyproline triplets, J. Biol. Chem. 282 (2) (2007) 1296–1304.
[22] A.D. Konitsiotis, N. Raynal, D. Bihan, E. Hohenester, R.W. Farndale, B. Leitinger, Characterization of high affinity binding motifs for the discoidin domain receptor DDR2 in collagen, J. Biol. Chem. 283 (11) (2008) 6861–6868.
[23] N. Kuznetsova, S. Leikin, Does the triple helical domain of type I collagen encode molecular recognition and fiber assembly while telopeptides serve as catalytic domains?: effect of proteolytic cleavage on fibrillogenesis and on collagen-collagen interaction in fibers, J. Biol. Chem. 274 (51) (1999) 36083–36088.
[24] S.T. Kreger, B.J. Bell, J. Bailey, E. Stites, J. Kuske, B. Waisner, S.L. Voytik-Harbin, Polymerization and matrix physical properties as important design considerations for soluble collagen formulations, Biopolymers 93 (8) (2010) 690–707.
[25] E.E. Antoine, P.P. Vlachos, M.N. Rylander, Review of collagen I hydrogels for bioengineered tissue microenvironments: characterization of mechanics, structure, and transport, Tissue Eng. B Rev. 20 (6) (2014) 683–696.
[26] G. Forgacs, S.A. Newman, B. Hinner, C.W. Maier, E. Sackmann, Assembly of collagen matrices as a phase transition revealed by structural and rheologic studies, Biophys. J. 84 (2) (2003) 1272–1280.
[27] J. Parkinson, K.E. Kadler, A. Brass, Simple physical model of collagen fibrillogenesis based on diffusion limited aggregation, J. Mol. Biol. 247 (4) (1995) 823–831.
[28] S. Rhee, J.L. Puetzer, B.N. Mason, C.A. Reinhart-King, L.J. Bonassar, 3D bioprinting of spatially heterogeneous collagen constructs for cartilage tissue engineering, ACS Biomater. Sci. Eng. 2 (10) (2016) 1800–1805.
[29] J. Pupkaite, M. Ahumada, S. McLaughlin, M. Temkit, S. Alaziz, R. Seymour, M. Ruel, I. Kochevar, M. Griffith, E.J. Suuronen, E.I. Alarcon, Collagen-based

photoactive agent for tissue bonding, ACS Appl. Mater. Interfaces 9 (11) (2017) 9265–9270.
[30] G. Tronci, C.A. Grant, N.H. Thomson, S.J. Russell, D.J. Wood, Multi-scale mechanical characterization of highly swollen photo-activated collagen hydrogels, J R Soc Interface 12 (102) (2015), 20141079-20141079.
[31] K.E. Drzewiecki, J.N. Malavade, I. Ahmed, C.J. Lowe, D.I. Shreiber, A thermoreversible, photocrosslinkable collagen bio-ink for free-form fabrication of scaffolds for regenerative medicine, Technology 5 (4) (2017) 185–195.
[32] N.S. Kajave, T. Schmitt, T.-U. Nguyen, V. Kishore, Dual crosslinking strategy to generate mechanically viable cell-laden printable constructs using methacrylated collagen bioinks, Mater. Sci. Eng. C 107 (2020), 110290.
[33] B. Sanz, A. Albillos Sanchez, B. Tangey, K. Gilmore, Z. Yue, X. Liu, G. Wallace, Light Cross-Linkable Marine Collagen for Coaxial Printing of a 3D Model of Neuromuscular Junction Formation, Biomedicines, 2021.
[34] Z. Wu, J. Liu, J. Lin, L. Lu, J. Tian, L. Li, C. Zhou, Novel digital light processing printing strategy using a collagen-based bioink with prospective cross-linker procyanidins, Biomacromolecules 23 (1) (2022) 240–252.
[35] H. Liang, S.J. Russell, D.J. Wood, G. Tronci, A hydroxamic acid–methacrylated collagen conjugate for the modulation of inflammation-related MMP upregulation, J. Mater. Chem. B 6 (22) (2018) 3703–3715.
[36] Y. Li, Q. Mao, X. Li, J. Yin, Y. Wang, J. Fu, Y. Huang, High-fidelity and high-efficiency additive manufacturing using tunable pre-curing digital light processing, Addit. Manuf. 30 (2019).
[37] C.R. Wittmer, J.A. Phelps, W.M. Saltzman, P.R. Van Tassel, Fibronectin terminated multilayer films: protein adsorption and cell attachment studies, Biomaterials 28 (5) (2007) 851–860.
[38] N. Diamantides, L. Wang, T. Pruiksma, J. Siemiatkoski, C. Dugopolski, S. Shortkroff, S. Kennedy, L.J. Bonassar, Correlating rheological properties and printability of collagen bioinks: the effects of riboflavin photocrosslinking and pH, Biofabrication 9 (3) (2017), 034102.
[39] A.R. Yousefi, K. Ako, Controlling the rheological properties of wheat starch gels using Lepidium perfoliatum seed gum in steady and dynamic shear, Int. J. Biol. Macromol. 143 (2020) 928–936.
[40] B. Zakani, D. Grecov, Yield stress analysis of cellulose nanocrystalline gels, Cellulose 27 (16) (2020) 9337–9353.
[41] X. Zhang, L. Xu, S. Wei, M. Zhai, J. Li, Stimuli responsive deswelling of radiation synthesized collagen hydrogel in simulated physiological environment, J. Biomed. Mater. Res. 101A (8) (2013) 2191–2201.
[42] L. Ouyang, R. Yao, Y. Zhao, W. Sun, Effect of bioink properties on printability and cell viability for 3D bioplotting of embryonic stem cells, Biofabrication 8 (3) (2016), 035020.
[43] D. Therriault, S.R. White, J.A. Lewis, Rheological behavior of fugitive organic inks for direct-write assembly, Appl. Rheol. 17 (1) (2007), 10112-1-10112-8.
[44] G. Gillispie, P. Prim, J. Copus, J. Fisher, A.G. Mikos, J.J. Yoo, A. Atala, S.J. Lee, Assessment methodologies for extrusion-based bioink printability, Biofabrication 12 (2) (2020), 022003.
[45] B. Leitinger, Discoidin Domain Receptor Functions in Physiological and Pathological Conditions, (1937-6448 (Print)).
[46] B. Leitinger, Molecular analysis of collagen binding by the human discoidin domain receptors, DDR1 and DDR2: identification of collagen binding sites in DDR2, J. Biol. Chem. 278 (19) (2003) 16761–16769.
[47] K. Saha, A.J. Keung, E.F. Irwin, Y. Li, L. Little, D.V. Schaffer, K.E. Healy, Substrate modulus directs neural stem cell behavior, Biophys. J. 95 (9) (2008) 4426–4438.
[48] C. Palumbo, R. Massa, M. Panico, A. Di Muzio, P. Sinibaldi, G. Bernardi, A. Modesti, Peripheral nerve extracellular matrix remodeling in Charcot-Marie-Tooth type I disease, Acta Neuropathol. 104 (3) (2002) 287–296.
[49] N.G. Carri, K. Rubin, D. Gullberg, T. Ebendal, Neuritogenesis on collagen substrates. Involvement of integrin-like matrix receptors in retinal fibre outgrowth on collagen, Int. J. Dev. Neurosci. 10 (5) (1992) 393–405.
[50] S. Yoshii, M. Oka, Peripheral nerve regeneration along collagen filaments, Brain Res. 888 (1) (2001) 158–162.
[51] L. Zhang, T. Yuan, L. Guo, X. Zhang, An in vitro study of collagen hydrogel to induce the chondrogenic differentiation of mesenchymal stem cells, J. Biomed. Mater. Res. 100A (10) (2012) 2717–2725.
[52] B. Cao, J. Li, X. Wang, Z. Ran, J. Tan, L. Deng, Y. Hao, Mechanosensitive miR-99b mediates the regulatory effect of matrix stiffness on bone marrow mesenchymal stem cell fate both in vitro and in vivo, APL Bioeng. 7 (1) (2023), 016106.
[53] G.Y. Li, S. Fukunaga, K. Takenouchi, F. Nakamura, Comparative study of the physiological properties of collagen, gelatin and collagen hydrolysate as cosmetic materials, Int. J. Cosmet. Sci. 27 (2) (2005) 101–106.